Structural and magnetic properties of NiMnSb/InGaAs/InP(001)

A. Koveshnikov, G. Woltersdorf, J. Q. Liu, B. Kardasz, O. Mosendz, B. Heinrich, and
K. L. Kavanagh[a]
Department of Physics, Simon Fraser University, Burnaby, BC V5A 1S6 Canada

P. Bach, A. S. Bader, C. Schumacher, C. Rüster, C. Gould, G. Schmidt, and
L. W. Molenkamp
Experimentelle Physik III, Universität Würzburg, Am Hubland, 97074 Würzburg, Germany

C. Kumpf
Experimentelle Physik II, Universität Würzburg, Am Hubland, 97074 Würzburg, Germany

The structural and magnetic properties of NiMnSb films, 5–120 nm thick, grown on InGaAs/InP(001) substrates by molecular-beam epitaxy, were studied by x-ray diffraction, transmission electron microscopy (TEM), and ferromagnetic resonance (FMR) techniques. X-ray diffraction and TEM studies show that the NiMnSb films had the expected half-Heusler structure, and films up to 120 nm were pseudomorphically strained at the interface, greater than the critical thickness for this system, about 70 nm (0.6% mismatch to InP). No interfacial misfit dislocations were detected up to 85 nm, however, relaxation in the surface regions of films thicker than 40 nm was evident in x-ray reciprocal space maps. TEM investigations show that bulk, planar defects are present beginning in the thinnest film (10 nm). Their density remains constant but they gradually increase in size with increasing film thickness. By 40 nm these defects have overlapped to form a quasicontinuous network aligned closely with ⟨100⟩ in-plane directions. The associated strain fields and or compositional ordering from these defects introduced a reduction in crystal symmetry that influenced the magnetic properties. The in-plane and perpendicular FMR anisotropies are not well described by bulk and interface contributions. In thick films, the in-plane uniaxial and fourfold anisotropies increased with increasing film thickness. The lattice defects resulted in a large extrinsic magnetic damping caused by two-magnon scattering, an increase in the coersive field with increasing film thickness, and a lower magnetic moment (3.6 Bohr magnetons) compared to the expected value for the bulk crystals (4 Bohr magnetons). © *2005 American Institute of Physics.*
[DOI: 10.1063/1.1873036]

I. INTRODUCTION

NiMnSb is a cubic, half-metallic, ferromagnetic alloy that is of interest for spintronics applications. Its high Curie temperature (730 K) means that it is potentially useful for the injection of spin-polarized charge into a semiconductor at room temperature. Towards this goal, it has been grown epitaxially by molecular-beam epitaxy (MBE) onto GaAs(001),[1] GaAs(111)B,[2] and InP/InGaAs (001) substrates.[3] However, the demonstration of a high degree of spin polarization at a surface or interface of this material has yet to be reported.

The defect structure, and stoichiometry of the bulk film and surfaces may hold the key to optimal magnetic properties and successful spin transport. The lattice constant for the stoichiometric phase grown epitaxially on GaAs has been reported to range between 0.5904 and 0.5909 nm,[1] and therefore, there is a larger lattice mismatch with GaAs compared to InP, 4.4% vs 0.6%. Pseudomorphic films in compression have been successfully grown on InP using an InGaAs buffer layer,[3] whereas the GaAs film interfaces would have been heavily dislocated.

In this paper, we investigate in greater detail the structural and magnetic properties of NiMnSb films grown epitaxially on oriented InP/InGaAs(001) substrates.[3] Although the films are indeed single crystalline, they contain a dense array of bulk structural defects that influence their strain and magnetic properties.

II. EXPERIMENTAL PROCEDURES

Samples were grown in an interconnected, multichamber, MBE system consisting of a Riber 2300 system for III-V, and a MBE-Komponenten GmbH system for the NiMnSb growths. The substrates were epiready, InP(Fe) (001) wafers (<0.2° misorientation) that were preheated in an UHV degassing chamber at 300 °C for 10 min prior to entry into the III-V chamber. The oxide was then desorbed under an As_4 overpressure by heating at 20 K/min until the (2×4) InP reconstruction was observed by reflection high-energy electron diffraction (RHEED). The substrate was then stabilized to the InGaAs growth temperature (typically 510 °C), and an InGaAs buffer (typically 200 nm) was grown (In to Ga flux ratio of 3.2 and an As flux $25 \times$ the group III total). After the growth of the buffer layer the sample was transferred to the NiMnSb growth chamber where NiMnSb was deposited at a substrate temperature of 300 °C as determined from the thermocouple in the sample holder. The three elements Ni, Mn,

[a] Electronic mail: kavanagh@sfu.ca

97, 073906-1

and Sb were simultaneously evaporated onto the (3×4) reconstructed (In,Ga)As surface. The flux ratios were set to 14.3 and 2.4 for Sb to Ni and Mn to Ni, respectively. Growth was started by simultaneous evaporation of all the three materials. After typically 2 monolayers $(ML = a_0/2)$ a sharp and streaky RHEED pattern appeared which stayed this way throughout the entire growth. The growth rate was calibrated using RHEED oscillations and was set to typically 0.1 ML/s. From the RHEED oscillations it was concluded that NiMnSb grows in the Franck–Van der Merwe growth mode, which results in high crystalline quality. Analysis of low-energy electron diffraction (LEED) spot profiles indicated that the surface steps were predominantly $a_0/2 = 0.294$ nm rather than $a_0/4$. Experiments showed that the (2×1) surface reconstruction was due to a Mn/Sb termination rather than Ni, such that NiMnSb antiphase boundaries were not expected. Further details about the growth can be found in Ref. 3.

The samples to be discussed in this paper were grown at the optimal substrate temperature (300 °C), in a series with NiMnSb thicknesses ranging from 5 to 120 nm. In some cases a Ti layer (5 nm) was deposited on the surface to reduce oxidation after removal from the UHV system. This Ti layer did not have an effect on the transmission electron microscopy (TEM) results. In order to determine the strain state of the NiMnSb layers, grazing incidence reciprocal space maps (RSMs) around the (353) Bragg reflection were measured at the BW2 beamline of the Hamburger Synchrotronstrahlungslabor (HASYLAB) at DESY using a wavelength of 1.24 Å (10 keV). Additionally, the interface uniformity and the average thickness of each sample were determined by the x-ray diffraction (XRD) measurements at a standing-anode diffractometer.

Plan-view samples for TEM were prepared by chemically dissolving the InP substrate in concentrated HCl leaving the InGaAs/NiMnSb intact. Cross sections were prepared by focused ion-beam (FIB) sectioning (30-keV Ga ion beam). TEM was carried out at an electron-beam accelerating voltage of 200 keV. Ferromagnetic resonance (FMR) was measured at 24 or 36 GHz, with the static magnetization in

TABLE I. The sample properties, the NiMnSb nominal thickness, and corresponding symbols used in Figs. 7, 8, and 10 are defined.

Sample	Thickness (nm)	Ti cap (5 nm)	Magnetic measurement symbols (Figs. 7, 8, and 10)
1	5	Yes	Filled square
2	10	Yes	Open circle
3	15	No	Filled triangle up
4	20	Yes	Open triangle down
5	30	Yes	Filled diamond
6	40	No	Filled triangle right
7	40	No	X-ray space map
8	42	Yes	Open triangle left
9	70	No	X-ray space map
10	85	No	Open star
11	120	No	X-ray space map

and out of the film plane configuration, at room temperature.[4] The magnitude of the longitudinal magneto-optic Kerr effect (MOKE) was measured along in-plane $\langle 110 \rangle$ directions. Superconducting quantum interference device (SQUID) magnetometry was used to determine the magnetic moment.

III. RESULTS

Table I gives a list of the samples and their thicknesses investigated in this paper. X-ray measurements reported earlier[3] using rocking curve analysis found 90-nm-thick NiMnSb films to be pseudomorphically strained, with narrow (004) linewidths (12 arc sec) and sharp interfaces. Figure 1 shows (353) reciprocal space maps for 40-, 70-, and 120-nm thick NiMnSb films. The maps represent cuts through reciprocal space in the plane defined by $(hkl) = [h, (5/3)h, l]$, i.e., a plane spanned by the direction normal to the surface and the (350) in-plane vector. It therefore contains information about the relaxation state of the NiMnSb layer in both lateral and vertical directions. The largest peak at $(h, l) = (3, 3)$ [corresponding to $(hkl) = (353)$] is from the lattice matched InP/InGaAs. The second peak directly below,
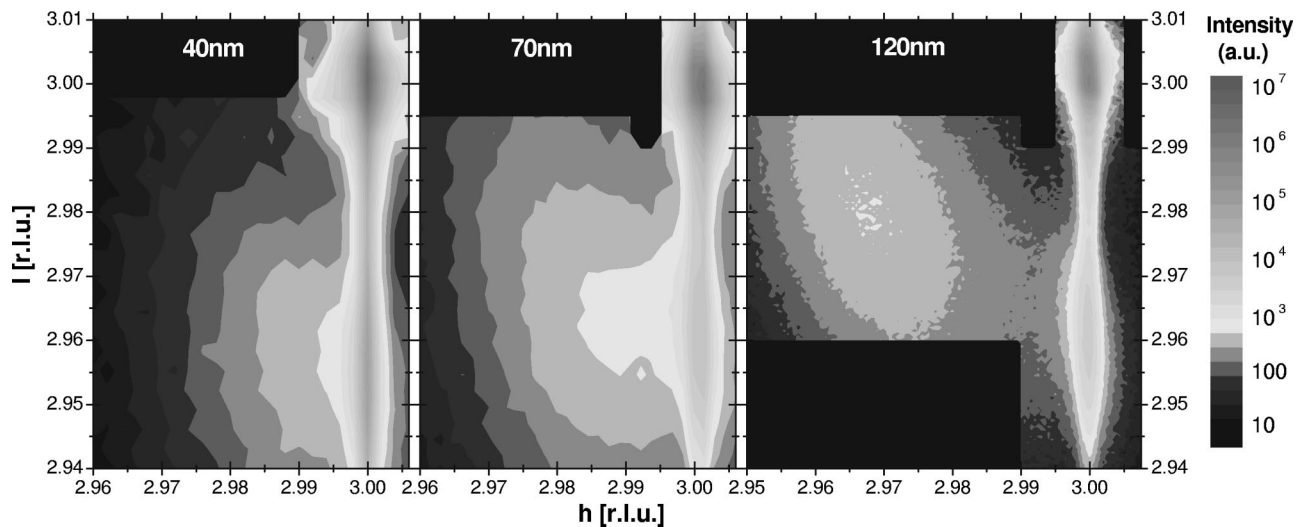

FIG. 1. Grazing incidence, x-ray reciprocal space maps (353) of NiMnSb/InGaAs/InP(001) samples as a function of NiMnSb film thickness (samples 7, 9, and 11, Table I).
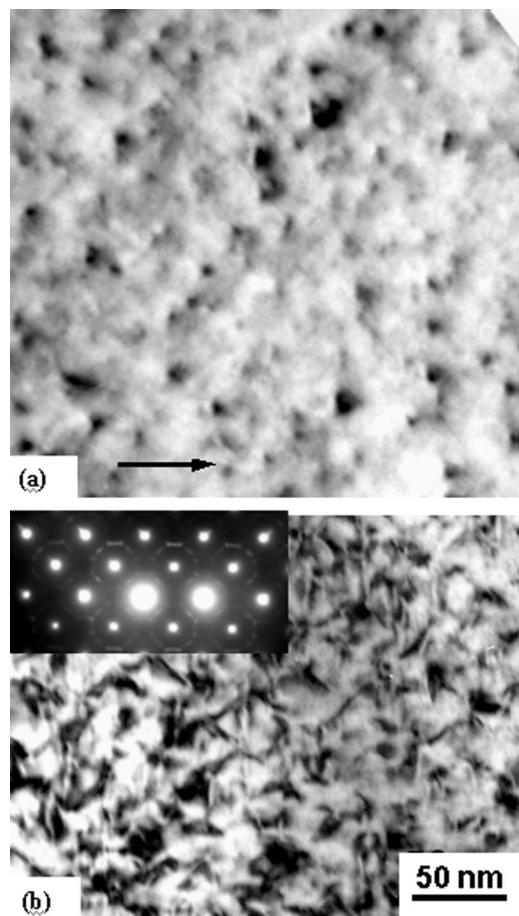
FIG. 2. Transmission electron microscopy, bright field images of NiMnSb/InGaAs(001) films obtained with the beam perpendicular to the film surface (plan-view) for two NiMnSb film thicknesses (a) 10 nm and (b) 40 nm (samples 2 and 6, Table I). The film has been tilted to a strong, two-beam, diffraction condition, diffraction vector $\mathbf{g}=(220)$, as indicated by the arrow in (a) and the selected area diffraction (SAD) pattern in (b). (See Fig. 3. for an indexed SAD.)
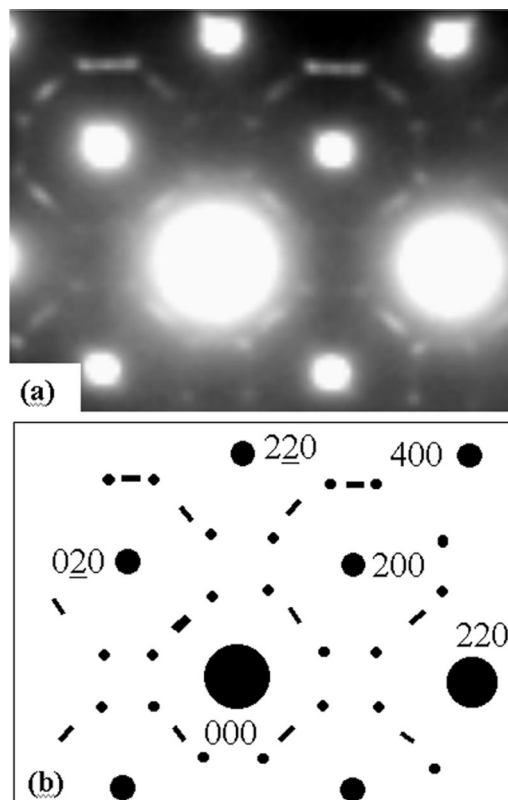

FIG. 3. The selected area diffraction pattern in Fig. 2 has been magnified in (a) and indexed in the diagram in (b). The major spots are regular diffraction from the expected NiMnSb/InGaAs structures, while the weaker, extra streaks and spots are from NiMnSb ordering along the $\langle 100 \rangle$ and $\langle 110 \rangle$ directions.

$(h,l) \approx (3,2.96)$, stems from the pseudomorphic NiMnSb layer. The lateral position of this peak $(h=3)$ is identical to that of the InP bulk, which indicates a laterally compressed unit cell for the NiMnSb layer. According to this data, the unit cell of the layer is expanded vertically causing a vertical shift of the Bragg peak to a position of $l \approx 2.96$, below the bulk peak position. For a layer thickness of 70 nm a third peak is detected, shifting to a position of $(h,l) \approx (2.975,2.975)$. This stems from the material having the relaxed (cubic) NiMnSb lattice parameter and indicates that relaxation occurs in the NiMnSb layer above thicknesses between 40 and 70 nm. Hence, there are two regions of the film with different strain states in this case. From a variation of the beam absorption depth with incidence angle it was determined that it was the surface regions of the film that were no longer pseudomorphic.[5]

In agreement with the XRD results the TEM measurements showed that the NiMnSb films were single crystalline. However, isolated defects were found beginning in the thinnest film (10 nm) investigated. These increased in size with increasing film thickness until they appeared to overlap by 40 nm. Figure 2 shows plan-view TEM micrographs for 10- and 40-nm NiMnSb/InGaAs films and an associated selected

area diffraction (SAD) pattern of the 40-nm film. These are bright field (BF) images both obtained with the sample tilted to a strong diffraction condition indicated by the diffraction vector, the arrow in the figure; in this case $\mathbf{g}=(220)$. Defects are visible with a density of $1 \times 10^3 \ \mu m^{-2}$ or average spacing of 30 nm. It is apparent that these defects are forming early in the growth likely at the interface and then growing larger with thickness, overlapping by 40 nm. Their density did not increase with thickness. The strong spots in the diffraction pattern are consistent with a NiMnSb half-Heusler alloy composition combined with the zinc-blende InGaAs.[1] (An in-plane lattice mismatch of the magnitude expected here would not be detectable from spot splitting in the diffraction patterns even if there had been interfacial strain relaxation.) Figure 3(a) shows a higher magnification image of the SAD in Fig. 2(b) with an indexed diagram in (b). Weak half-order streaks at $\frac{1}{2}(200)$ are apparent along each $\langle 100 \rangle$ direction with associated superlattice spots along perpendicular $\langle 100 \rangle$ directions. There are also indications of streaks aligned along $\langle 110 \rangle$ directions at an approximate index of $(1/\sqrt{2})(220)$, which intersect those in the $\langle 100 \rangle$ directions. This extra diffraction indicates that atomic scale ordering exists in the NiMnSb. Streaks rather than sharp spots indicate that the ordering occurs in planar domains aligned closely with the $\langle 100 \rangle$ and $\langle 110 \rangle$ directions.

To investigate the defects further, Fig. 4 shows the BF images from the same area of a 40-nm NiMnSb film, tilted to $\mathbf{g}=(220)$, $(2\underline{2}0)$, (200), and (020) diffraction conditions as
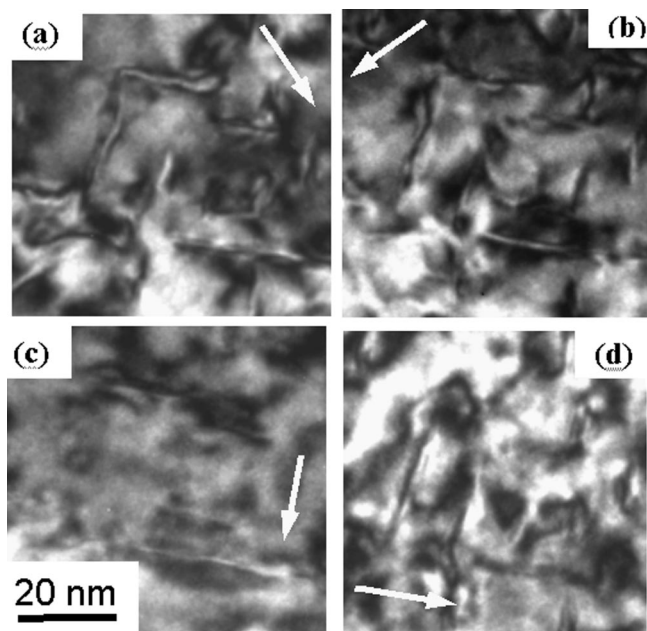
FIG. 4. Transmission electron microscopy, bright field images of a NiMnSb(001) film (40 nm) as in Fig. 2. An identical area is imaged as a function of diffraction conditions (sample tilted), as indicated by the arrows perpendicular to the diffraction planes (a) (220), (b) (2$\bar{2}$0), (c) (200), and (d) (020). In this region, the InGaAs substrate has been etched away. The dotted white arrow indicates the same defect in each image.
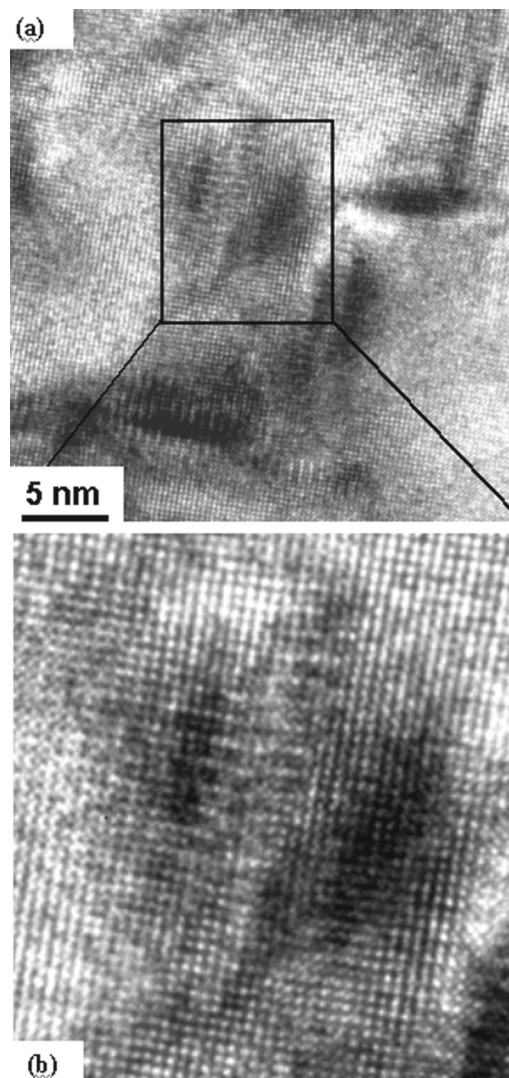

FIG. 5. The same film as in Fig. 4 imaged in plan view, downpole (parallel to the [001] direction) at higher magnification, using multiple beams showing interference fringes from the (002) planes in each material. Image (b) is a magnified view by a factor 3 of the square area in (a).

indicated by the arrow. The predominant contrast is from the defects aligned close to the $\langle 100 \rangle$ directions. These are still visible under $\{220\}$ diffraction conditions, whereas most go out of contrast for the perpendicular $\{200\}$ condition. This indicates that there is little lattice displacement parallel to the defect line direction, consistent with either an edge dislocation or a stacking fault.[6] The defects when in contrast appear with a black/white/black appearance or as single black regions depending on the degree of deviation from the exact Bragg condition. Another set less prominent in this region but clear in Fig. 3(b) are aligned with the $\langle 110 \rangle$ directions and go completely out of contrast for either the $\{200\}$ diffraction conditions or the $\mathbf{g} = [2\bar{2}0]$ condition perpendicular to its line direction. Tilting this sample by large angles (up to 20°) about in-plane $\langle 110 \rangle$ axes caused an increase in the length of the $\langle 110 \rangle$ defects, indicating that they are inclined to the film interface.

Along the edges of the thinned regions of the same sample, thinner patches were found where the InGaAs layer had been etched away leaving only NiMnSb [confirmed by scanning transmission electron microscopy (STEM) energy dispersive x-ray analysis]. There was no difference in the density of defects observed but without the InGaAs, the films were much more transparent and the lattice images were clearer. Figure 5(a) shows a multibeam, lattice image example obtained with the electron beam parallel to the [001] pole. The smallest, square lattice fringes have a spacing of 0.30 ± 0.01 nm, thus associated with the $\{200\}$ NiMnSb planes. The magnified view in (b) shows one isolated defect but a Burger's circuit around the defect showed that there were no dislocations with lines intersecting the surface in this area.[6] The surrounding crystal is in phase. However, in-

side the defect region there is clearly an extended deformation with double-period fringes visible along the defect length consistent with $\{100\}$ ordering. There also appears to be a double stacking fault with many distortions perpendicular to the long direction. In some cases, the double fringe regions extended out parallel to the $\langle 110 \rangle$ directions but there were no isolated defects aligned with that direction.

The thickest films investigated by TEM (85 nm), show overlapping, planar defects aligned approximately with in-plane $\langle 120 \rangle$ directions, as shown in Fig. 6(a). Atomic ordering is still visible in the SAD. Figure 6(b) shows a cross-sectional, phase contrast, TEM image from the same sample, taken with the electron-beam direction aligned with the $\langle 110 \rangle$ direction. The NiMnSb/InGaAs interface is abrupt and atomically smooth. The (002) fringe spacing on each side of the interface measures 0.29 ± 0.01 nm (InGaAs) and 0.30 ± 0.01 nm (NiMnSb). The lattice constant for InP is 0.5868 nm (2×0.292 nm^2) so the InGaAs and the NiMnSb films are closely matched but slightly in compression consistent with the x-ray results. It was not possible to tell from
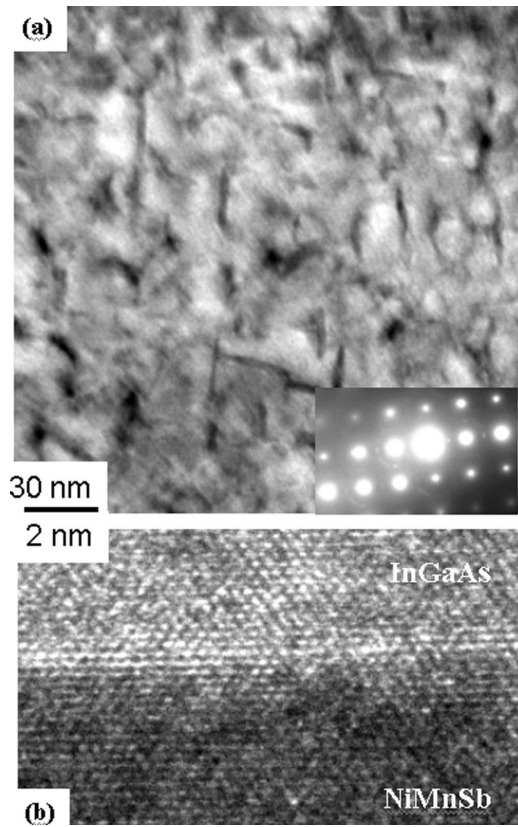
FIG. 6. Plan view (a) and cross sectional (b) view of an 85-nm-thick NiMnSb/InGaAs film (sample 10, Table I) obtained with transmission electron microscopy. The insert in (a) is a selected area diffraction pattern showing the diffraction conditions and orientation of the film. The defects appear to align closely with the $\langle 120 \rangle$ directions as well as the $\langle 100 \rangle$.

this thinned sample whether there were any interfacial dislocations or other defects at the interface since the perpendicular fringes were unclear.

The FMR field (corresponding to the maximum in rf losses) H_{FMR} in the NiMnSb(001) as a function of in-plane angle φ of the applied field, with respect to the [100] crystallographic axis, is shown in Fig. 7. (The graphed symbols associated with each sample are listed in Table I). These data indicate a strong variation of H_{FMR} with the film thickness and in-plane angle φ. Furthermore, there is clearly a uniaxial component (repeating every 180°) in the thinnest and thickest films for the fields aligned along a $\langle 011 \rangle$ direction. The magnetic moment from the SQUID magnetometry of a 42-nm sample was found to be $3.6\mu_B$ at 4 K per NiMnSb unit formula. Magnetic hysteresis loops for 10-, 42-, and 85-nm films are shown in Fig. 8. With an increasing thickness the coercive field increased from 3 to 60 Oe.

IV. DISCUSSION

A. Structural properties

The exact nature of the defects remains unclear, however, interfacial (misfit) dislocations can be ruled out. The TEM images obtained using different diffraction conditions identified two sets of defects aligned approximately with the $\langle 100 \rangle$ and exactly with the $\langle 110 \rangle$ in-plane directions. The strong loss of contrast that we observed for each change in
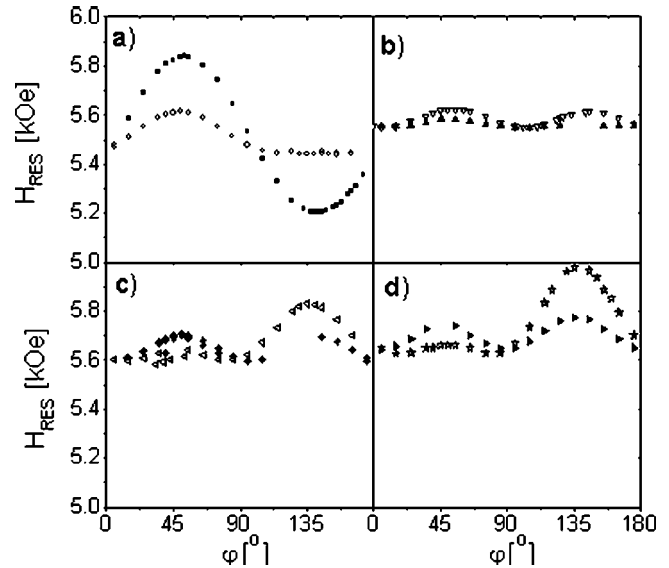

FIG. 7. Angular dependence of the maximum FMR field at 23.92 GHz as a function of sample thickness (nm) (a) 5 and 10, (b) 15 and 20 (c) 30 and 40, and (d) 42 and 85 (symbols are listed in Table I). The applied dc field and the saturation magnetization are in plane. The angle φ is in the direction of the applied field and the saturation magnetization with respect to the [100] crystallographic axis of NiMnSb(001). The accuracy is less than 0.5%.

the diffraction condition rules out dislocations with slip vectors out of the plane of the interface. For example, 60 ° dislocations, a common type of misfit dislocation found in lattice mismatched, semiconductor systems,[7] would remain in contrast under these diffraction conditions. Pure interfacial edge misfits with in-plane, slip vectors $\mathbf{b} = \frac{1}{2}\{110\}$ or $\frac{1}{4}\{100\}$, and glide planes perpendicular to the surface of the film could explain the TEM data. However, in that case the average spacing of the defects observed (30 nm) would have meant complete relaxation of the tetragonal strain in the film. The x-ray measurements found little strain relaxation in the thinner films, certainly up to 40-nm thicknesses, and at greater thickness the relaxation occurred in only the surface region of the NiMnSb. In addition, a comparison of images of the NiMnSb layer with and without the InGaAs layer found little difference in the defect densities, indicating that they are located in the bulk rather than at the interface. Fi-
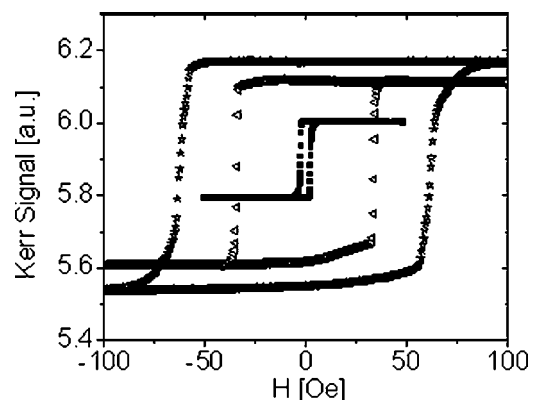

FIG. 8. The hysteresis loops for 5-, 40-, and 85-nm thick films (symbols listed in Table I). The hysteresis loops were carried out by using the longitudinal magneto-optic Kerr effect (MOKE) with the magnetic field along the in-plane easy axis [1$\underline{1}$0], [110], and [110] directions, respectively.
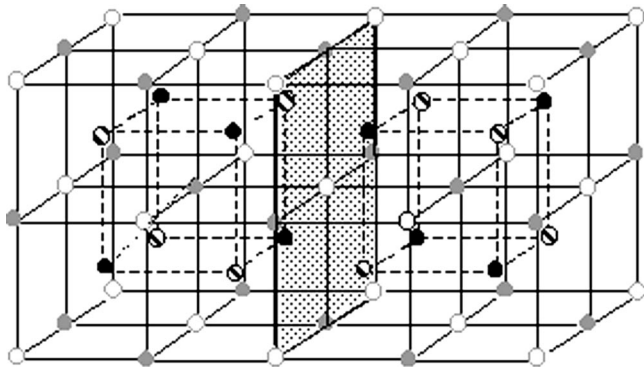
FIG. 9. Diagram showing an antiphase boundary plane formed by a 90° rotation in the Mn/Sb sublattice (Ni gray, vacancies white, Sb black, and Mn striped circles).

nally, the fact that tilting the sample caused changes in the length of the $\langle 110 \rangle$ defects indicates that they are inclined to rather than lying on the interface. The contrast observed along $\langle 110 \rangle$ may originate from dislocations but if so, these thread through the film.

The $\langle 100 \rangle$ defects are a collection of isolated planar defects running from the interface to the surface, which overlap in thicker films. They are not $\{111\}$ stacking faults, the defects that commonly occur in fcc cubic systems. These would have been easily identified in the low magnification plan-view images from the strong extinction fringes that are associated with them. Such relatively coarse fringes were not observed in these films. However, stacking faults on the planes perpendicular to the growth plane ($\{100\}$ or $\{110\}$) cannot be easily ruled out. These could be associated with the extended ordering domains clearly seen in the high magnification image, from the double-period, lattice fringes within the defect regions. A well-known type of stacking fault, called an antiphase boundary, typical of the growth of III-V semiconductors on group IV semiconductors, e.g., GaAs/Si or GaP/Si,[8,9] does not appear to be present, consistent with the conclusions from the RHEED and LEED measurements. These involve atoms from both sublattices and have a distinct contrast for different diffraction conditions. However, there is also the possibility of antiphase boundaries associated with only one sublattice, such as errors in the Mn and Sb atomic locations. Figure 9 shows a drawing of one such defect in the stacking of $\{100\}$ planes. Similar defects could also be imagined along $\{110\}$ and $\{120\}$ planes. Such imperfections might have influenced the subsequent Ni layer, generated threading dislocations, and could explain the ordering and contrast. If these defects were also responsible for the surface strain relaxation, then their effects would have been greatest in the thickest films, as was observed.

B. Magnetic properties

The FMR fields (Fig. 7) were fit with a model calculation that allows one to determine the magnitude of the magnetic anisotropies that exist in these films.[4] A combination of three components was identified, in-plane uniaxial-anisotropy field $2K_U^{\parallel}/M_s$, a fourfold in-plane anisotropy field $2K_1^{\parallel}/M_s$, and the field $4\pi M_{\text{eff}}$, which is required to magnetize the sample perpendicular to the surface, where M_s is the
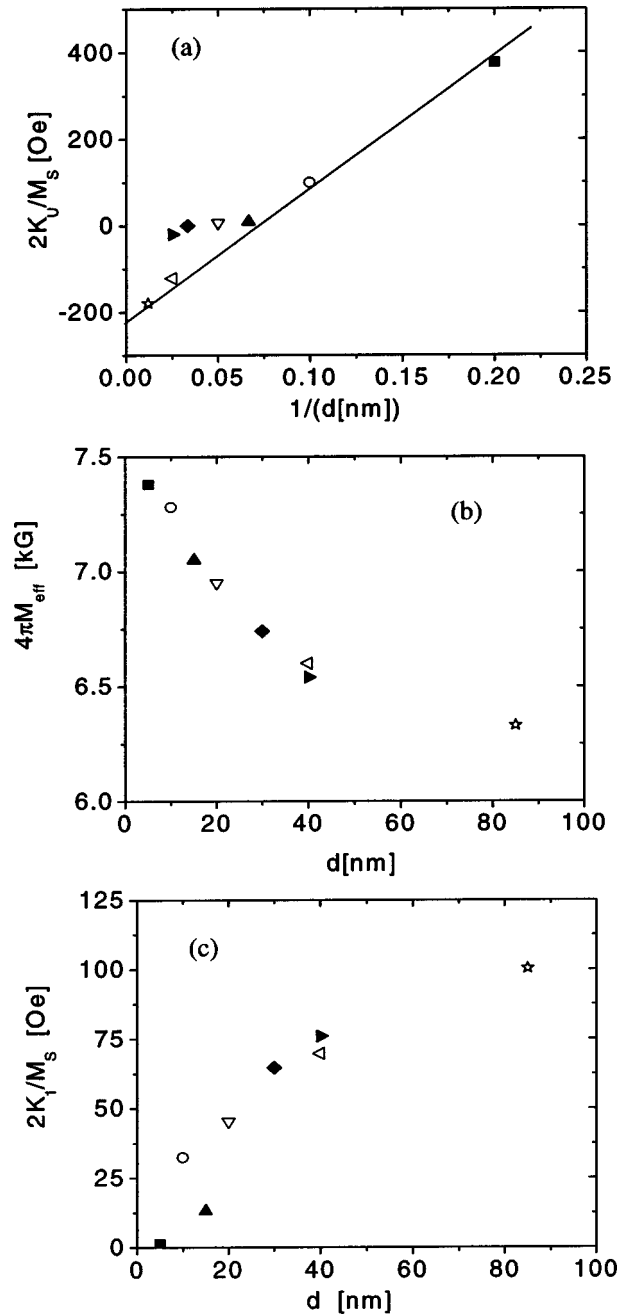

FIG. 10. The dependence of (a) the in-plane uniaxial-anisotropy field $2K_U/M_s$ as a function of $1/d$, (b) the in-plane fourfold anisotropy field $2K_1/M_s$ as a function of d, and (c) $4\pi M_{\text{eff}}$ as a function of d, where d is the NiMnSb(001) film thickness (symbols listed in Table I). Note that for plot (a) the films in the intermediate thickness range have nearly zero uniaxial anisotropy. The direction of the in-plane uniaxial-anisotropy axis is along the $[1\underline{1}0]$ direction with respect to the InP(001) template. Note that the coefficient of the in-plane uniaxial anisotropy changes its sign for the thickest samples.

saturation magnetization. $4\pi M_{\text{eff}} = 4\pi M_s - 2K_U^{\perp}/M_s$, where $2K_U^{\perp}/M_s$ is the perpendicular uniaxial anisotropy, which in cubic materials can arise either from interfaces or lattice strains. See a detailed discussion of magnetic anisotropies in Ref. 10. Figures 10(a)–10(c) show the analysis of the results in Fig. 7 for $2K_U^{\parallel}/M_s$, $4\pi M_{\text{eff}}$, and $2K_1^{\parallel}/M_s$ as a function of the film thickness d or $1/d$.

In the case of the in-plane anisotropy field $2K_U^{\parallel}/M_s$, the uniaxial axis was aligned with the $[1\underline{1}0]$ direction of the

InP(001) wafer. For the thinnest and thickest films there was a well-defined $1/d$ dependence (straight-line overlay), which could indicate the presence of an interface, in-plane uniaxial anisotropy $K_{U,s}^{\parallel}=0.08$ erg/cm^2 (magnetic easy axis). Its origin is most likely associated with the interface chemistry between the NiMnSb(001) film and the InGaAs(001) substrate. However, the asymptotic value of $K_{U,s}^{\parallel}$ $(d\rightarrow\infty)$ approaches -200 Oe. This anisotropy value can arise from an anisotropic relaxation of the in-plane tetragonal strain. Anisotropic strain relaxation along the crystallographic [110] and [1$\underline{1}$0] orientations from misfit dislocations was found in Fe/GaAs(001) films[11] and in Fe/InAs(001) films.[12] The resulting, in-plane shear strain (due to a larger strain relaxation along the [110] than along the [1$\underline{1}$0] direction) resulted in an appreciable in-plane uniaxial anisotropy in these cases, with the easy magnetic axis also along [1$\underline{1}$0]. In our samples the [1$\underline{1}$0] crystallographic direction is the easy uniaxial axis. Still unexplained is the absence of in-plane uniaxial anisotropy for intermediate thickness films [see Fig. 10(a)].

The results for $4\pi M_{\text{eff}}$ and $2K_1^{\parallel}/M_s$ [Figs. 10(b) and 10(c)] did not show a linear dependence as a function of $1/d$. The $4\pi M_{\text{eff}}$ gradually decreased while $2K_1^{\parallel}/M_s$ gradually increased with increasing film thickness. Both the distortion and asymmetry in the in-plane strain increased with increasing film thickness, associated with a reduction of crystal symmetry from tetragonal to at least orthorhombic but likely triclinic or monoclinic. The SQUID measurements for a 42-nm-thick film, at room temperature, resulted in $4\pi M_s$ $=7.42$ kG ($\pm$ 1% relative error), leading to $2K_U^{\perp}/M_s$ $=0.7$ kOe, with the easy axis parallel to the film normal. This also clearly indicates the presence of lattice strain. However, for other thicknesses we cannot be certain of the magnitude of the perpendicular uniaxial anisotropy. The fourfold component of the in-plane magnetic anisotropy $2K_1^{\parallel}/M_s$ increases with increasing thickness. It is interesting to note that $2K_1^{\parallel}/M_s$ is absent for the thinnest films. $2K_1^{\parallel}/M_s$ is most likely caused by the crystallographic defects satisfying the in-plane, fourfold symmetry. A similar behavior was observed in the ultrathin films of bcc Ni(001) grown on Fe(001) templates.[13]

The theoretical magnetic moment for NiMnSb is expected to be $4\mu_B$ (Ref. 14) and is observed in bulk samples.[15] The lower value of the magnetic moment [$3.6\mu_B$, $4\pi M_s$ $=8.17$ kG ($\pm$ 1% relative error)] observed at $T=4$ K in a 42-nm film is most likely caused by the growth-induced lattice defects which bring the minority-spin band below the Fermi surface.

Significant information can be obtained from the FMR linewidths. For the thinnest sample ($d=5$ nm), the lowest value of the FMR linewidth was 20 Oe at 24 GHz and was nearly independent of the angle φ. This isotropic FMR linewidth scaled linearly with the microwave frequency,[16] and therefore, the magnetic damping was caused by intrinsic Gilbert damping.[10] Intrinsic Gilbert damping in metals is caused by spin-orbit interactions.[17] In thin NiMnSb the measured Gilbert damping parameter has a remarkably low value, G $=3.1\times10^7$ s^{-1}, indicating that the role of spin-orbit interactions in the magnetic damping of NiMnSb is rather weak. The situation changes gradually with increasing film thick-

ness such that a tenfold increase in average ΔH was observed in the thickest film investigated, $d\sim85$ nm. Extrinsic damping processes due to magnetic inhomogeneities created by the defects and ordering domains presumably cause this gradual increase in ΔH. The out-of-plane dependence of ΔH (Ref. 15) has shown that additional FMR line broadening could be described by a two-magnon scattering mechanism.[18] The in-plane angular dependence of ΔH was found to be primarily isotropic, indicating that the film magnetic inhomogeneities have a strong isotropic distribution independent of the orientation of the magnetization with respect to the crystallographic axes. However, ΔH had also a noticeable fourfold anisotropy with the maximum ΔH, aligned with the $\langle 110 \rangle$, crystallographic axis. The amplitude of the fourfold anisotropy in ΔH was approximately 1/5 of the isotropic contribution. Our previous studies using the lattice strained Fe(001) films on Cu(001) and Pd(001) substrates indicate[19,20] that a part of the lattice defects in the NiMnSb(001) films follow the $\langle 100 \rangle$ directions, consistent with the TEM results.

The presence of the crystallographic defects also strongly affects the width of the magnetic hysteresis loops, as shown in Fig. 8. With increasing defect density the coercive field increased from 3 to 60 Oe. Further information on the magnetic properties of these films can be found in Ref. 16.

V. CONCLUSIONS

The structural and magnetic properties of epitaxial NiMnSb/InGaAs/InP films were investigated as a function of film thickness. The reciprocal space map measurements indicated coherent films up to a film thickness of 120 nm, but the surface regions of the films showed relaxation beginning in 40-nm films. These results were consistent with TEM plan-view investigations that detected no interfacial misfit dislocations up to at least 85 nm, slightly greater than the theoretical critical thickness, 70 nm. Instead, a set of defects with a uniform density gradually evolved, increasing in size with increasing film thickness. They originated at the interface as seen in the thinnest films investigated by TEM (10 nm). These defects were edgelike and aligned with both the {100} and {110} in-plane directions. The dominant set appeared to be a type of a planar defect associated with the {100} planes, ordering and stacking faults. Classical antiphase boundaries were not found consistent with the LEED and RHEED investigations of step types.

The magnetic properties fully support the TEM and XRD diffraction studies. With increasing film thickness the lattice defects in the NiMnSb(001) films became more prominent as they expanded in size and resulted in well-defined bulklike in- and out-of-plane uniaxial anisotropies and angular dependent two-magnon scattering. Clearly, the thicker NiMnSb(001) films grown by MBE on InGaAs/InP(001) develop a lower degree of symmetry.

[1]W. Van Roy, J. de Boeck, B. Brijs, and G. Borghs, Appl. Phys. Lett. **77**, 4190 (2000).

[2]W. Van Roy, M. Wojcik, E. Jedryka, S. Nadolski, D. Jalabert, B. Brijs, G. Borghs, and J. de Boeck, Appl. Phys. Lett. **83**, 4214 (2003).

[3]P. Bach *et al.*, Appl. Phys. Lett. **83**, 521 (2003); P. Bach, C. Rüster, C. Gould, C. R. Becker, G. Schmidt, and L. W. Molenkamp, J. Cryst. Growth **251**, 323 (2003).

[4]B. Heinrich, *Radio Frequency Techniques*, Ultrathin Magnetic Structures Vol. II, edited by B. Heinrich and J. A. C. Bland (Springer, Berlin, 1994).

[5]P. Bach, A. S. Bader, C. Rüster, C. Gould, G. Schmidt, L. W. Molenkamp, and C. Kumpf (unpublished).

[6]P. Hirsch, A. Howie, R. Nicholson, D. W. Pashley, and M. J. Whelan, *Electron Microscopy of Thin Films*, 2nd ed. (R. E. Krieger Publishing Co., Florida, 1977).

[7]R. S. Goldman, K. L. Kavanagh, H. H. Wieder, S. N. Ehrlich, and R. M. Feenstra, J. Appl. Phys. **83**, 5137 (1998).

[8]Ph. Komninou, J. Stoemenos, G. P. Dimitrakopulos, and Th. Karakostas, J. Appl. Phys. **75**, 143 (1994).

[9]D. Cohen and C. B. Carter, J. Microsc. **208**, 84 (2002).

[10]B. Heinrich and J. F. Cochran, Adv. Phys. **42**, 523 (1993).

[11]O. Thomas, Q. Shen, O. Schieffer, and P. Lepine, Phys. Rev. Lett. **90**, 017205 (2003).

[12]Y. B. Xu, J. Freeland, M. Tselepi, and J. A. C. Bland, Phys. Rev. B **62**, 1167 (2000).

[13]B. Heinrich, S. Purcell, J. Dutcher, K. B. Urquhart, J. F. Cochran, and A. S. Arrott, Phys. Rev. B **38**, 12879 (1988).

[14]R. DeGroot, F. Mueller, P. van Engen, and K. Bushow, Phys. Rev. Lett. **50**, 2024 (1983).

[15]L. Ritchie *et al.*, Phys. Rev. B **68**, 104430 (2003).

[16]B. Heinrich, G. Woltersdorf, R. Urban, O. Mosendz, G. Schmidt, P. Bach, L. W. Molenkamp, and E. Rozenberg, J. Appl. Phys. **95**, 7462 (2004).

[17]B. Heinrich, R. Urban, and G. Woltersdorf, J. Appl. Phys. **91**, 7523 (2002).

[18]R. Urban, B. Heinrich, G. Woltersdorf, K. Ajdari, K. Myrtle, J. F. Cochran, and E. Rozenberg, Phys. Rev. B **65**, 020402(R) (2002).

[19]Z. Celinski and B. Heinrich, J. Appl. Phys. **70**, 5935 (1991).

[20]G. Woltersdorf and B. Heinrich, Phys. Rev. B **69**, 184417 (2004).